Bioinspired Porous Heterogeneous Aerogel Fibers with Woven Architecture for Ultra-Broadband Microwave Absorption and Thermal Regulation

*Zizhao Ding[a], Yiting Zhu[a], Tengxiao Mu [a], Shenglong Huang[a], Yilun Cheng[a], Dou Zhang[a], Zixiang Zhao[a], Zuojuan Du[a], Chao Jiang[a]**

[a]Powder Metallurgy Research Institute, State Key Laboratory of Powder Metallurgy, Central South University, Central South University, Changsha, 410083, People's Republic of China

Corresponding Author

*E-mail addresses: jiangchao@csu.edu.cn

1. Experimental Section

1.1 Materials

Potassium permanganate ($KMnO_4$) was procured from Aladdin Company. Graphite (1000 mesh) was purchased from Shenzhen Guoheng Qihang Technology Co., Ltd. Sodium nitrate ($NaNO_3$), nitric acid, sulfuric acid, 3,3′,4,4′-biphenyldicarboxylic acid (BPDA), p-phenylenediamine (PDA), triethylamine (TEA), and N-methyl-2-pyrrolidone (NMP) were obtained from Sinopharm Chemical Reagent Co., Ltd. All chemical reagents were of analytical grade and used without further purification. Deionized water was prepared in-house with a resistivity of approximately 18.5 MΩ·cm.

1.2 Synthesis of MoS_2@H-$MnFe_2O_4$

Manganese ferrite was synthesized via a chemical co-precipitation method. First, 20 mmol $MnCl_2·4H_2O$ and 40 mmol $FeCl_3·6H_2O$ were completely dissolved in 120 mL ethylene glycol under magnetic stirring. Then, 5 g urea and 1.2 g polyvinylpyrrolidone (PVP) were added and stirred until fully dissolved. The solution was transferred into a hydrothermal autoclave and reacted at 200 °C for 2 h. The product was washed and dried to obtain hollow $MnFe_2O_4$. Separately, 3 g sodium molybdate and 4.4 g thiourea

were dissolved in a 1:1 (v/v) ethanol-water solvent mixture. The as-prepared hollow $MnFe_2O_4$ was dispersed in this solution, followed by a hydrothermal treatment at 180 °C for 20 h. The black product was washed and dried, yielding MoS_2@H-$MnFe_2O_4$, denoted as MH.

1.3 Synthesis of PAAS

A total of 100 mL N-methyl-2-pyrrolidone (NMP) was added to a 250 mL three-neck flask, followed by 3.78 g (≈0.035 mol) of PDA crystals. Under a nitrogen atmosphere, the mixture was mechanically stirred until complete dissolution. Subsequently, an equimolar amount of BPDA powder was added. The reaction was carried out under mechanical stirring in an ice-water bath for 12 h to yield a transparent, viscous poly (amic acid) (PAA) solution with a solid content of 12 wt%. Finally, 10 mL TEA (≈0.070 mol) was introduced, and stirring was continued for another 4 h to obtain the poly(amic acid) ammonium salt (PAAS) solution.

1.4 Preparation of the Spinning Suspension

The FMHG spinning suspension was prepared by adding 265 mg graphene oxide (GO, synthesized via Hummers' method) and an equal mass of MH to 10 mL of the PAAS solution. For comparison, the FHG suspension was obtained by adding 265 mg GO and hollow $MnFe_2O_4$ (without MoS_2 shell) to the PAAS solution, while the FMH suspension was prepared by adding MH without GO.

1.5 Preparation of FMHG Aerogel Fibers and Fabric

First, the spinning suspension was loaded into a syringe to prepare FMHG composite fibers. The coagulation bath consisted of an acetic acid aqueous solution. The suspension was continuously extruded through a 20-gauge needle into the rotating coagulation bath. The as-formed fibers were collected, frozen, and freeze-dried for 24 h. The dried fibers were then subjected to thermal treatment at 300 °C for 2 h under a nitrogen atmosphere. Aerogel fibers with different diameters could be obtained by using needles of different gauges. Finally, the composite fibers were woven into a fabric with a warp density of 50 ends per 5 cm and a weft density of 30 ends per 5 cm^2.

1.6 Test Methods and Simulation Conditions

The intrinsic electromagnetic parameters of the aerogel were obtained by testing a

coaxial ring (inner diameter 3 mm, outer diameter 7 mm) made from aerogel fibres using a vector network analyzer. For the simulation of surface energy loss and electromagnetic field distribution in aerogel fiber fabrics, we employed a three-layer aerogel fabric, with each layer having a fiber thickness of 1 mm. the electromagnetic parameters of the fibers were taken from the intrinsic electromagnetic parameters measured in the coaxial test; the rear surface of the fabric was modelled as a perfect electrical conductor (PEC), whilst the remaining surfaces were treated as open (radiating) boundaries.

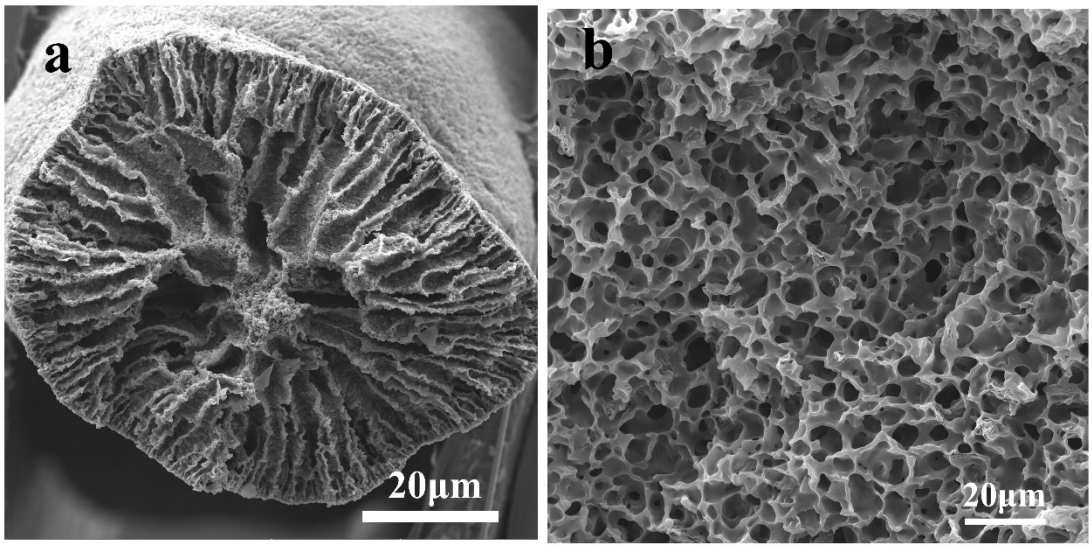

Figure S1 SEM image of FMHG aerogel fibers

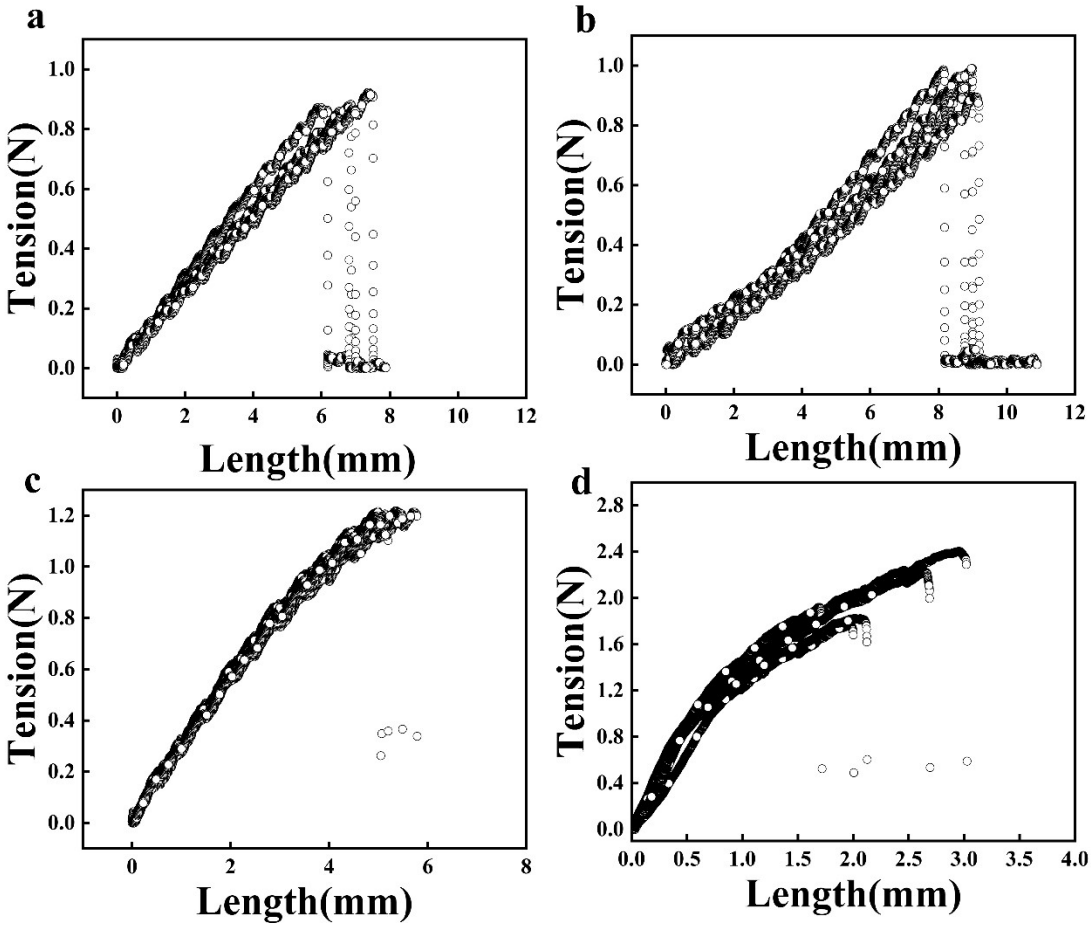

Figure S2 (a) FMH, (b) FHG, (c) FMHG-0.5, (d) FMHG-0.8.

For an all-dielectric microwave absorption system, the conditions of quarter-wavelength theory (Eq. (1)) and impedance matching (Eq. (2)) should be fulfilled to achieve the ideal broadband microwave absorption. Wu et al. obtained an ideal variation law for the dielectric constant by solving Eqs. (1) and (2), and the results are shown in Eqs. (S2) and (S3).

$$\varepsilon' = \frac{L_1^n}{(d \times f)^2} \quad (2)$$

$$\varepsilon'' = \frac{L_2^n}{(d \times f)} \quad (3)$$

Here L_1^n and L_2^n are constants, when n=0, L_1^n=5617.3GHz2mm2, L_2^n=95.28GHzmm.

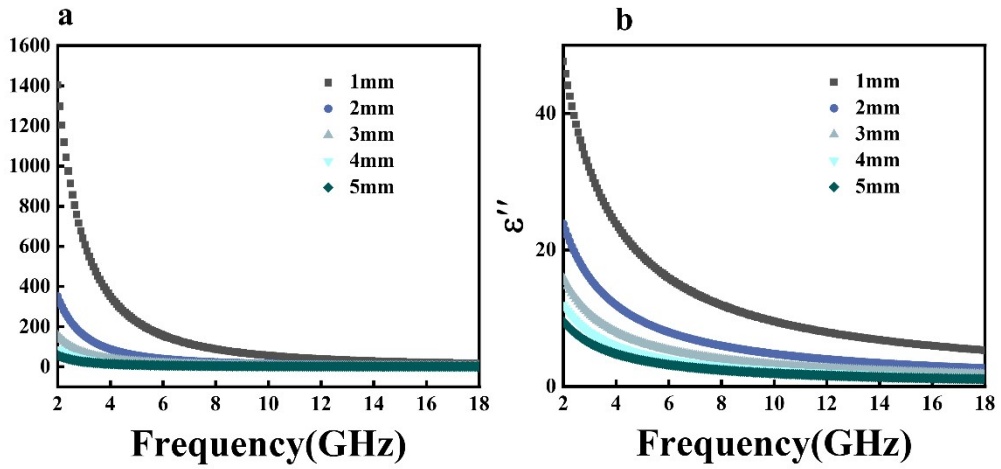

Figure S3. The change curves of the real (a) and imaginary (b) parts of the permittivity with frequency calculated according to the ideal permittivity equation.

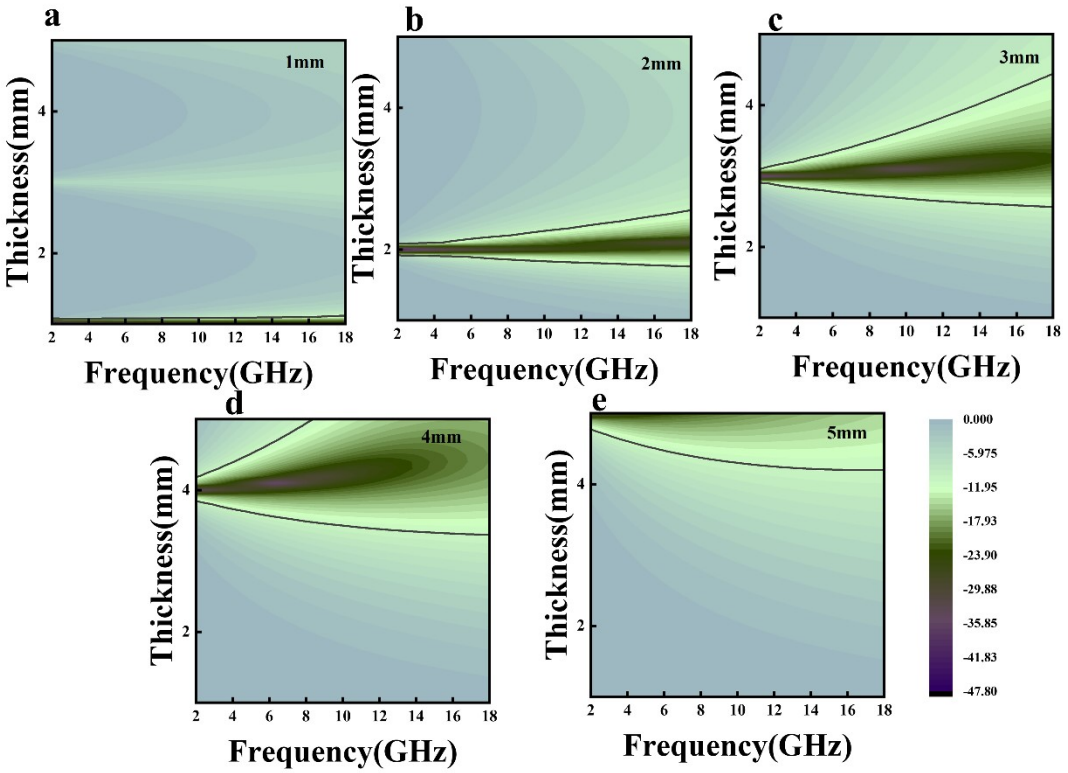

Figure S4. The microwave absorption performance at different thickness calculated by the ideal permittivity: (a) 1mm; (b) 2mm; (c) 3mm, (d) 4mm and (e) 5mm.

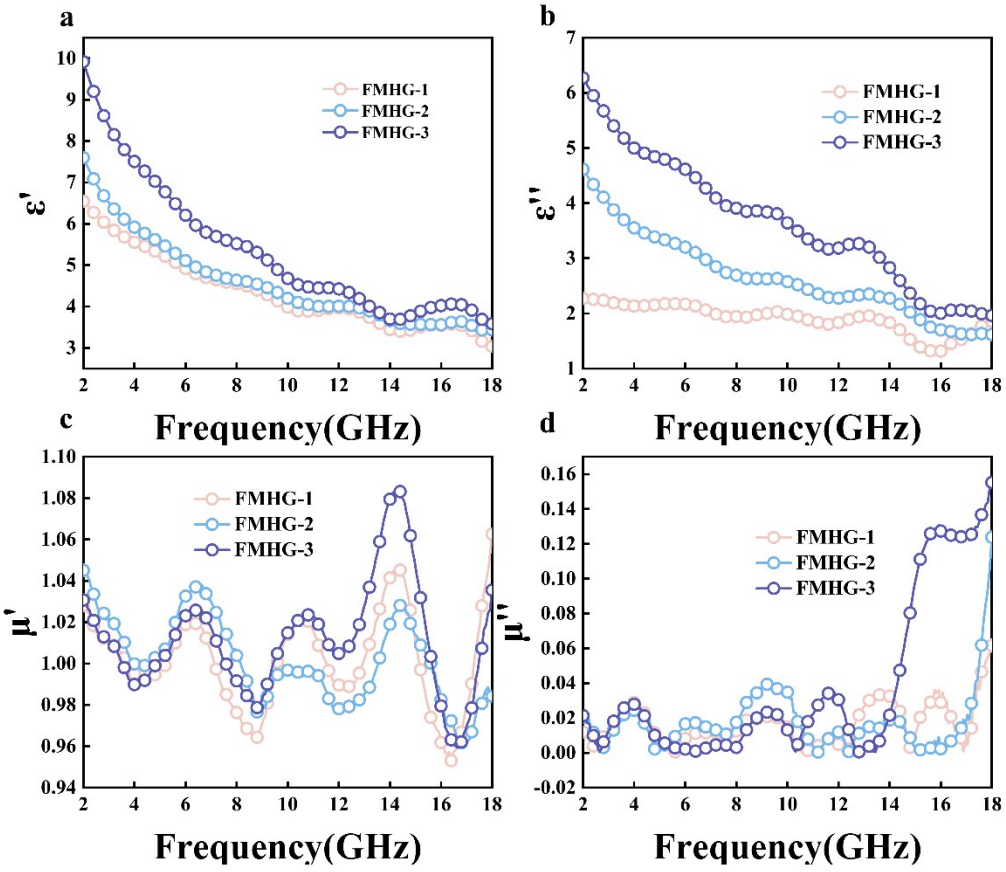

Figure S5 (a) Real part of dielectric constant, (b) Imaginary part of dielectric constant, (c) Real part of magnetic permeability, (d) Imaginary part of magnetic permeability.

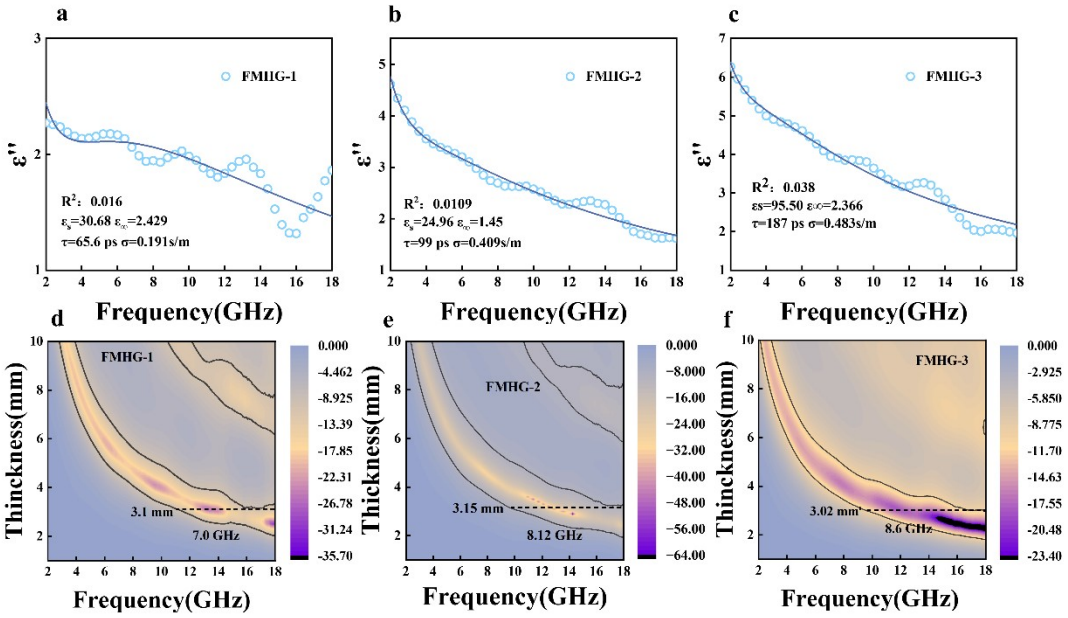

Figure S6 (a) Debye fitting for FMHG-1, (b) Debye fitting for FMHG-2, (c) Debye fitting for FMHG-3, (d) Effective absorption bandwidth for FMHG-1, (e) Effective

absorption bandwidth for FMHG-2, (f) Effective absorption bandwidth for FMHG-3.

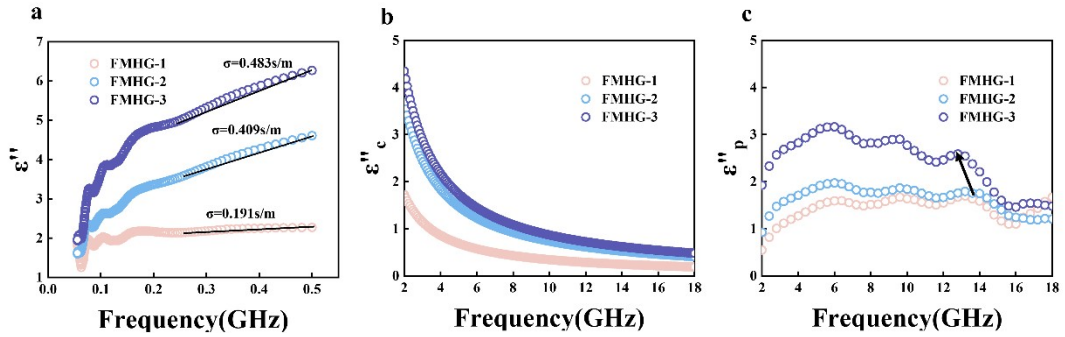

Figure S7 (a) Conductivity fitting of FMHG aerogel fibers, (b) Conductive loss of FMHG aerogel fibers, (c) Polarization loss of FMHG aerogel fibers.

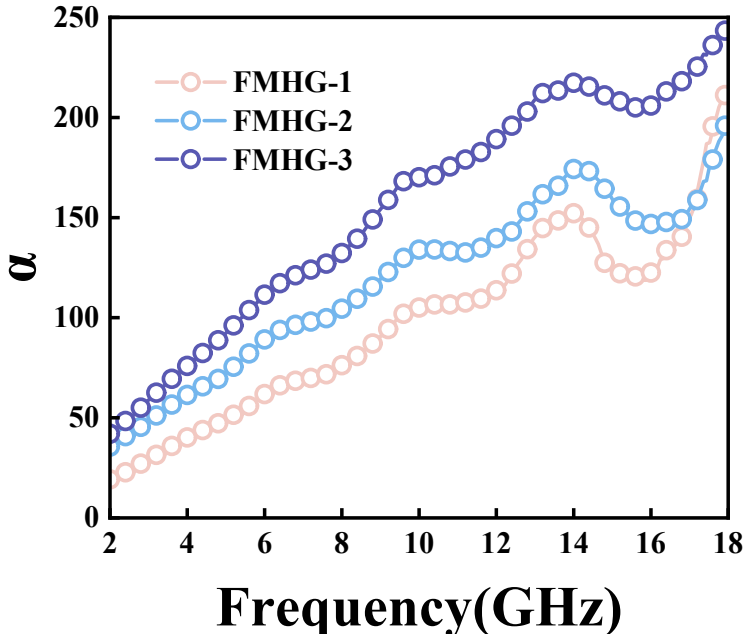

Figure S8 Damping constant of FMHG

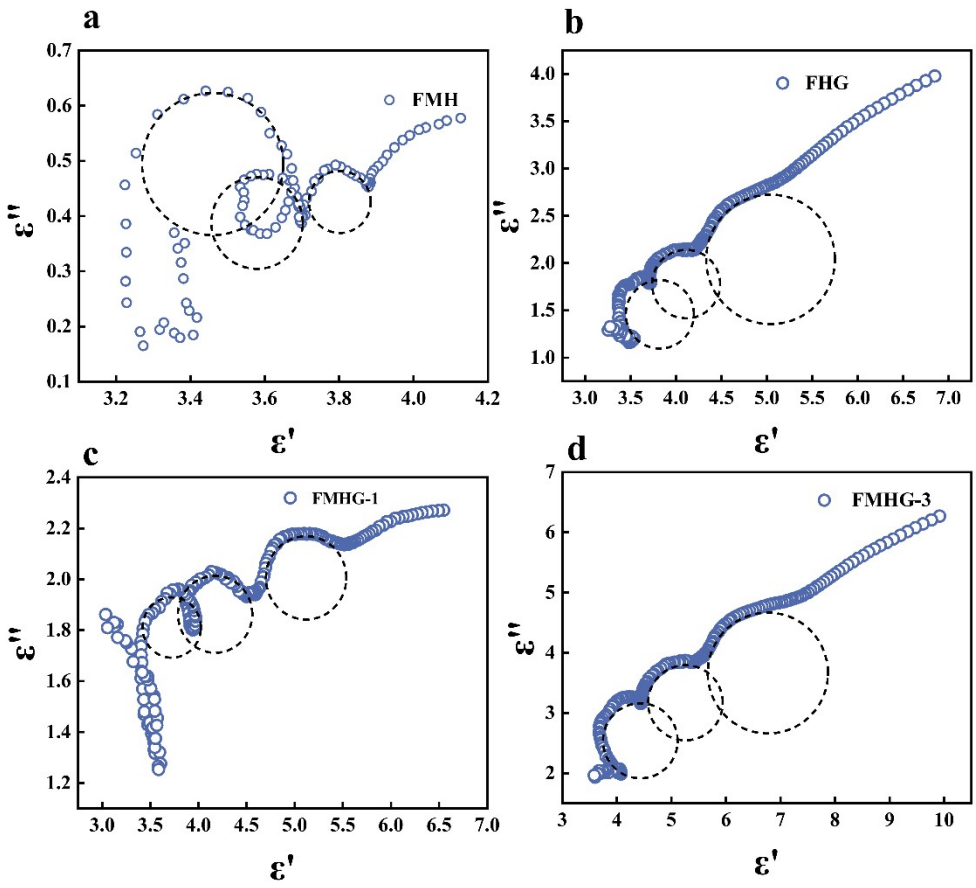

Figure S9 Cole-Cole diagram (a) FMH, (b) FHG, (c) FMHG-1, (d) FMHG-3.

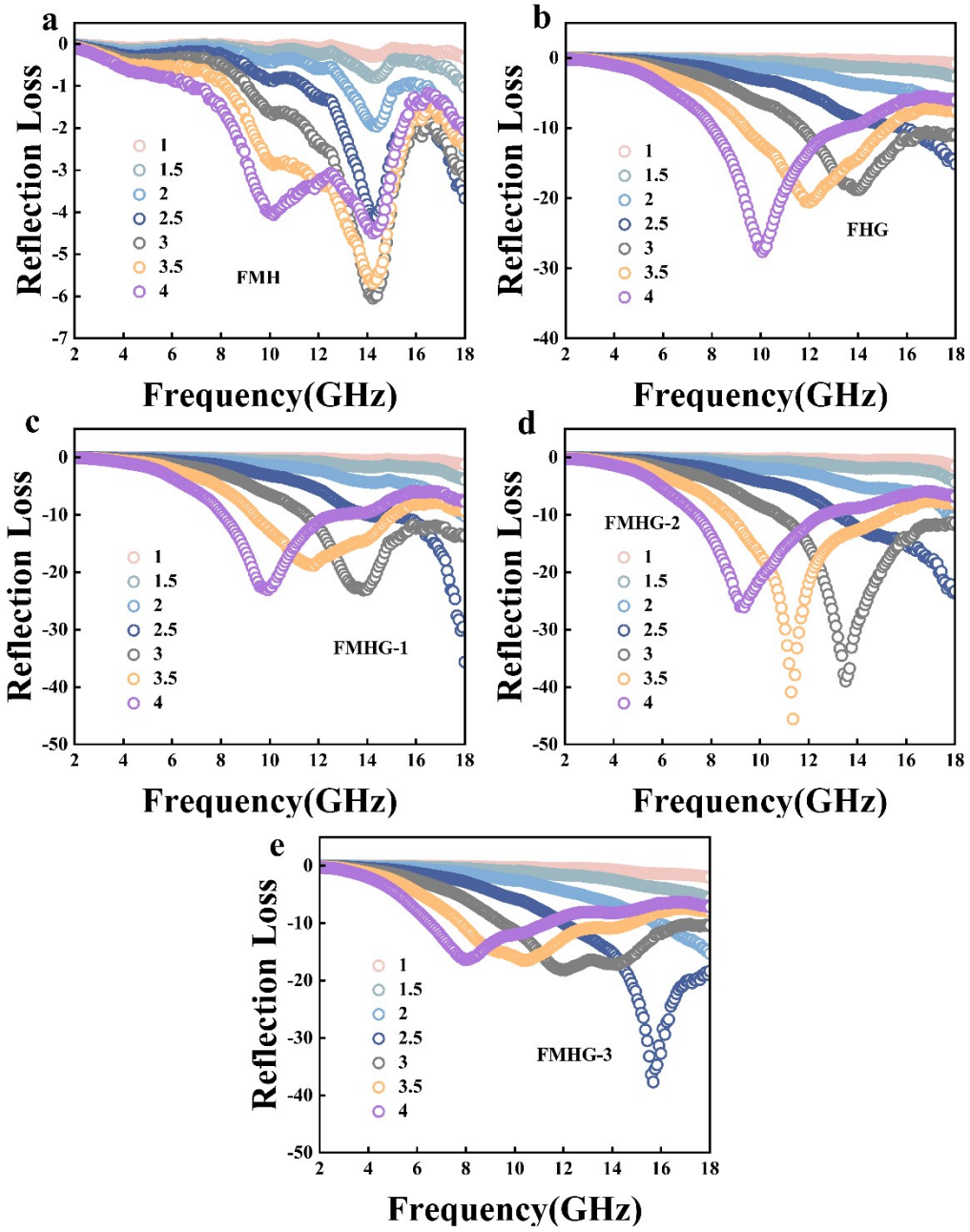

Figure S10 Absorption performance (a) FMH, (b) FHG, (c) FMHG-1, (d) FMHG-2, (e) FMHG-3.

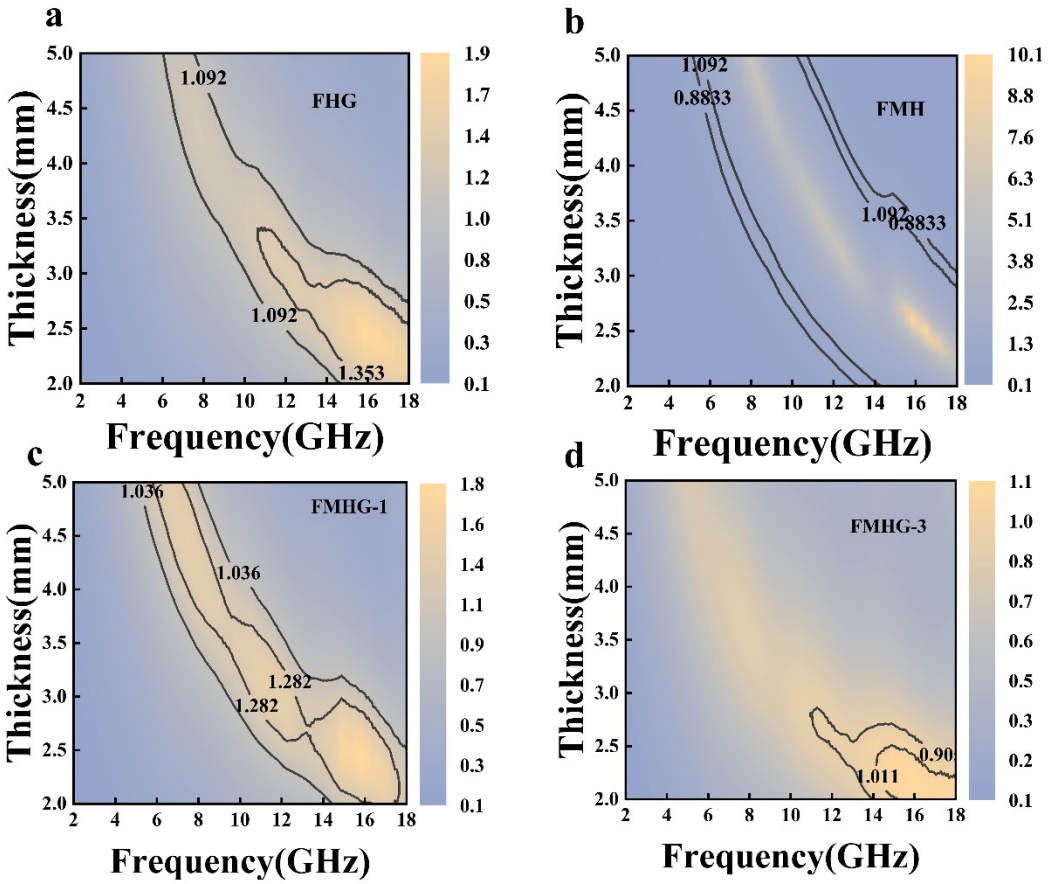

Figure S11 Impedance matching: (a) FHG, (b) FMH, (c) FMHG-1, (d) FMHG-3.

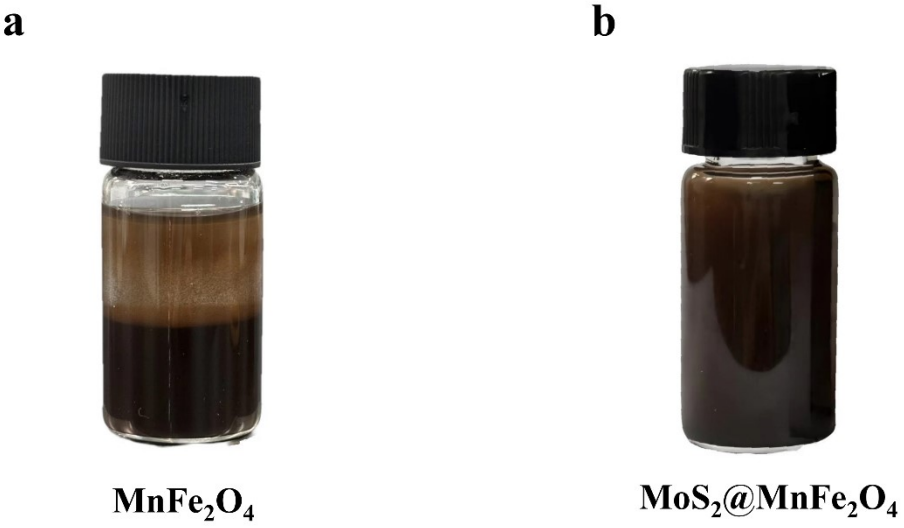

Figure S12 Solution state after 24 hours of dispersion.

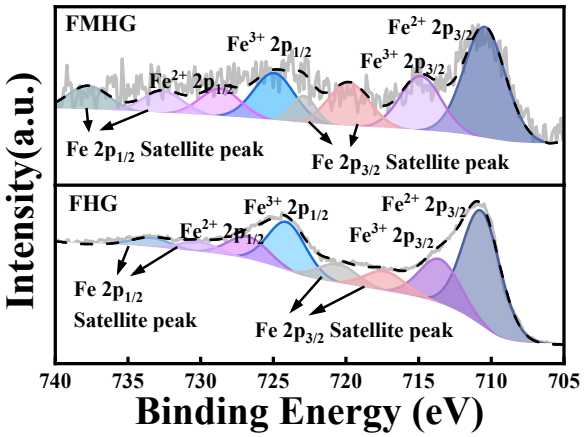

Figure S 13 Fe XPS fine spectrum.

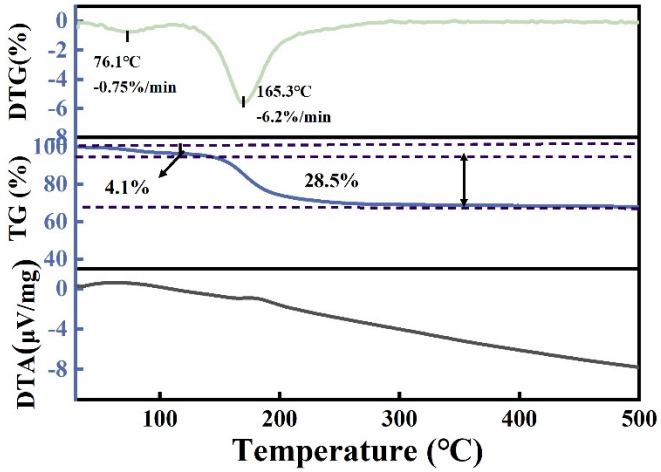

Figure S 14 FMHG's DTA curve.

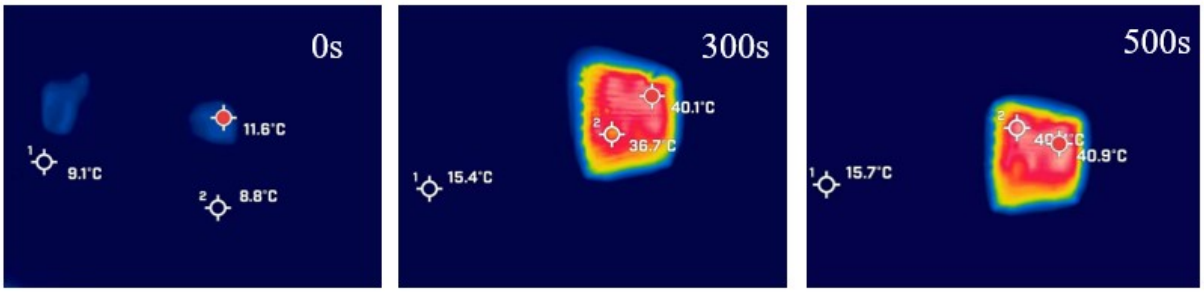

Figure S 15 The photoconversion capability of FMHG in humid environments.

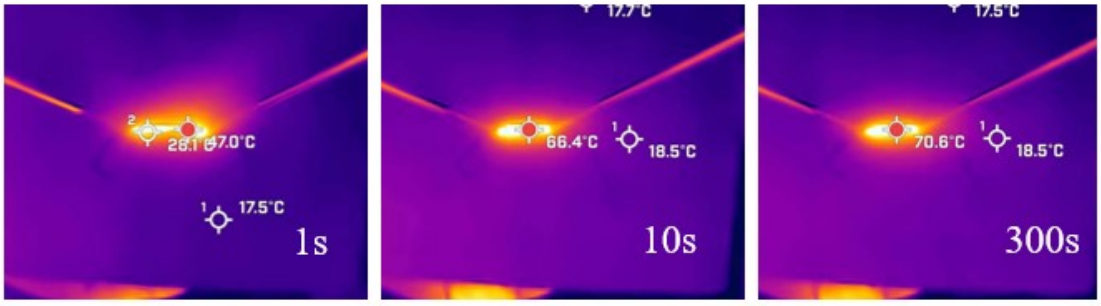

Figure S 16 The electrothermal conversion capability of FMHG in humid environments.

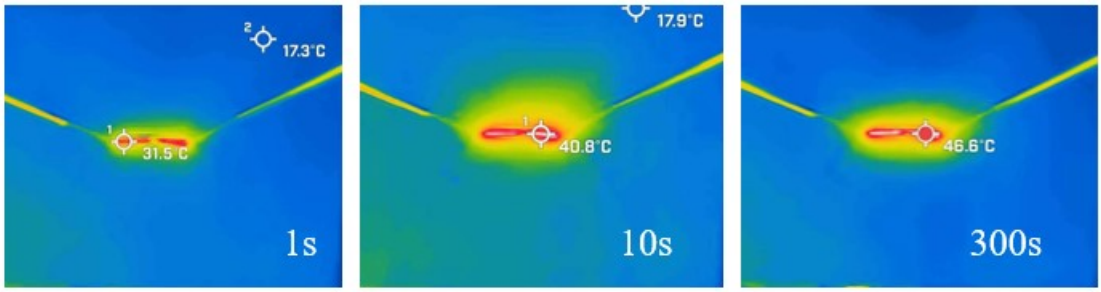

Figure S 17 The electrothermal conversion capability of FMHG after 100 folding cycles.

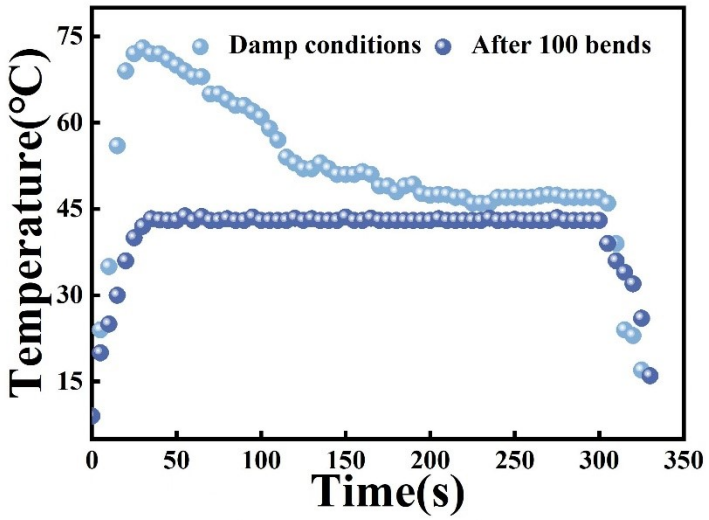

Figure S 18 Temperature versus time curve in a humid environment after 100 bending cycles.

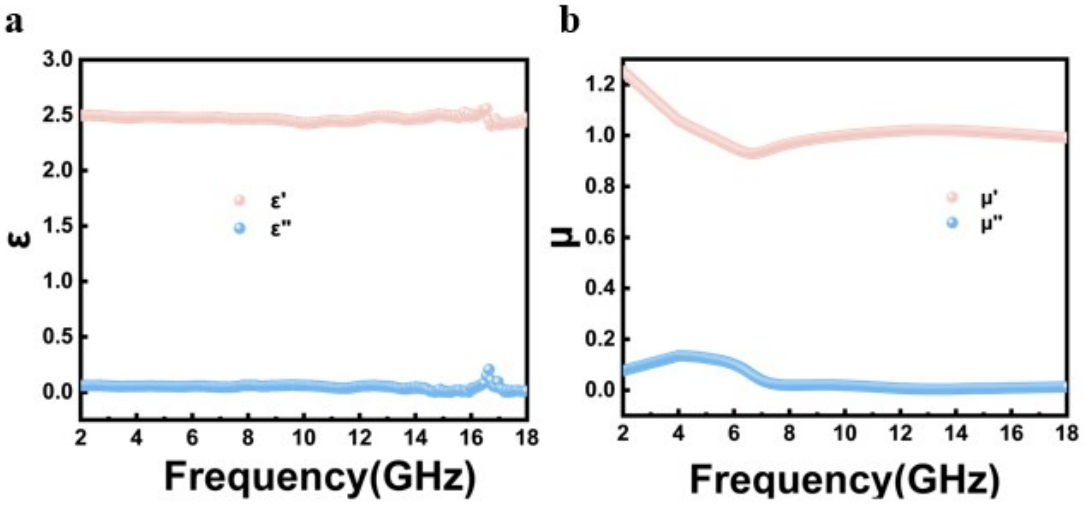

Figure S 19 Electromagnetic properties of PI aerogel fibers.

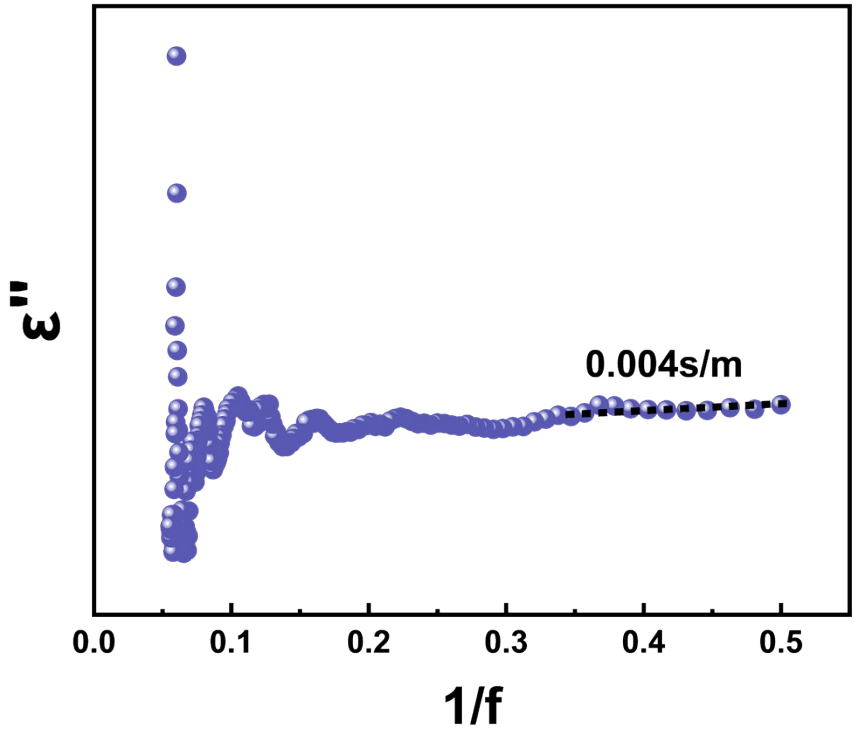

Figure S 20 Fitting the electrical conductivity of PI aerogel fibers.